UNIVERSITY of CALIFORNIA
SANTA CRUZ

ATOMIC INTERACTIONS: THERMAL, MAGNETIC AND TRANSPORT PROPERTIES OF PD_2TIIN_X $(0.87 \leq X \leq 1.22)$

A thesis submitted in partial satisfaction of the
requirements for the degree of

BACHELOR OF SCIENCE

in

PHYSICS

by

Jessica Missaghian

June 2011

The thesis of Jessica Missaghian is approved by:

Arthur P. Ramirez Advisor	Zack Schlesinger Advisor
Adriane Steinacker Senior Theses Coordinator	David P. Belanger Chair, Department of Physics

Abstract

Atomic Interactions: Thermal, Magnetic and Transport Properties of Pd_2TiIn_x

$(0.87 \leq x \leq 1.22)$

by

Jessica Missaghian

My work in a discovery driven research group led under the direction of Arthur P. Ramirez, Andrew LaForge and Zack Schlesinger explores the fundamentals of magnetic materials. Pd_2TiIn a polycrystalline inter-metallic compound with a face-centered cubic Heusler $L2_1$ structure has prompted interest and discussion over the past 20 years for its bulk magnetic properties and disputed magnetically ordered state. Prompted by scientific interest in weakly itinerant magnets and possible device applications motivated further research on Pd_2TiIn's electronic structure as well as an investigation into the nature of Heusler type alloys, magnetic order and the role of spin fluctuations. I present a comprehensive investigation into a series derived from Pd_2TiIn_x, $0.87 \leq x \leq 1.22$ by studying the magnetic, transport and heat capacity properties in the range from 2 - 300K.

Contents

List of Figures

List of Tables

To

Sharareh Hedvat & Maman Touran

با تشکر از شما برای مراقبت از عشق و حمایت شما
من شما را دوست دارم

To those who find awe in the natural world.

May you learn about the earth

through any school of thought or experience possible.

This thesis is but one way in which I have understood the beauty of being.

Acknowledgements

Arthur P. Ramirez, for sharing your knowledge and time, offering me a hands-on experience and teaching me practical lab skills and proper data analysis. Our weekly lunch meetings were invaluable to me as a learning experience. Zack Schlesinger, for the opportunity to work in a laboratory, and for many talks that inspired thought and inquiry. Andrew LaForge, for your patience in teaching me everything I ever needed to know about a low temperature physics lab. I am grateful for the time, effort and care you put into our work. Gey-Hong Gweon, for an inspiring course in Solid State physics. Your lectures inspired and framed my thinking for my senior thesis. Kelsey Collier, Garret Grogen and Dave Matthews for your help in carrying out the experiments. Callie Oglesby for making the samples studied in this thesis. Theo Seigrist and Andhika Kiswandhid for taking the time to do x-ray diffraction measurements. The UCSC library, for being my home away from home, without the books, librarians and online resources this thesis would not have been possible. My beautiful, loud and outrageous family, thank you for your unyielding love and support.

1

Introduction

"All things are made of atoms - little particles that move around in perpetual motion, attracting each other when they are a little distance apart, but repelling upon being squeezed into one another." As described by Richard Feynman the atomic postulate, in his opinion, encompasses the most information about scientific knowledge to date. With a little thinking and imagination astounding fundamental ideas can be extracted from that one sentence. In fact, matter can be understood through development of this atomic theory. The study of atoms, and therefore matter is a basis with which physicists have been able to understand the world around us. Matter is all around us. We interact with matter everyday using all of our senses. Amazingly though, matter is unfamiliar in many ways.

Materials have interested many peoples. Historically, ages of human existence have been defined by materials. In the paleolithic age materials such as copper, bronze and steel revolutionized lifestyles of tribes and hunter - gatherers. In more modern times prominent materials such as plastics, ceramics, composites and superconductors have brought about a new digital age. The 2010 Nobel Prize was given to two condensed matter physicists who

were able to produce a novel material, a single layer of carbon, Graphene. These materials have had a large impact on our understanding of matter and on the evolution of technology and devices. The propulsion of interest in materials and their applications has created an interdisciplinary field, Materials Physics, a discipline at the cross section of chemistry, condensed matter and physics.

Greek philosophers of the 6^{th} century B.C. first proposed the discontinuous nature of matter. Our ideas on atoms and the components of matter have evolved with time. The macroscopic properties of a material are understood through the small scale atomic interactions. These atoms are in perpetual motion, varying in degree depending upon the state of the material. In the gaseous state the atoms move at high velocities. They are chaotic and occupy a large volume. In contrast, when a material is in its solid state the atoms oscillate about a single point in a confined manner. In the solid state of matter the atoms sit on well defined points creating patterns often referred to as the lattice. In most materials the lattice exhibits symmetry and is a defining characteristic of the crystal. These structures can take on many geometries and configurations. It is surprising to think that most of the solids that we interact with on a day to day basis are actually crystals! In this "solid" state of matter there is a plethora of exotic and interesting physics that has become a hot field in the sciences.

For my senior thesis I will present a comprehensive research experiment on measured physical and magnetic properties of several metallic crystals. I will also give a review of basic principles in solid state physics to help put my work into context.

1.1 Models of Solid State Physics

By studying the periodic table one will notice that about $\frac{2}{3}$ of the elements are metals. The elements seem to favor the metallic state, characterized by the materials' conductivity, malleability and lustrous appearance. By studying metals we do not limit our understanding of other materials [Ashcroft and Mermin, 1976]. Understanding metallic compounds gives insight into other nonmetallic states.

In 1897 J. J. Thompson discovered the electron, and it was not until the early 20^{th} century that electrons were described by their particle-wave like nature. The cooperative behavior of the electrons in matter are the way in which we understand solids [Gweon, 2010]. Solid State Physics deals with the microscopic interactions between a few electrons and the macroscopic consequences of those interactions. So, in order to understand matter, from a physics point of view, it necessary to apply theories from quantum mechanics for the small scale phenomena and classical mechanics for the whole ensemble. To understand the physical properties of the simplest metals we can apply a few simple models: the Free Electron Theory Model and the Nearly Free Electron approximation. Both approximations make unintuitive assumptions, but both predict accurate behavior for many materials.

1.1.1 The Free Electron Model

In the Free Electron Model the valence electrons, electrons in the outermost orbitals of an atom, are given up to become conduction electrons. These itinerant electrons can be thought of as nomads, in perpetual motion, drifting, so they no longer belong to any specific atoms, and they are able to move freely throughout the material. In this model the electron-

electron interactions due to the Coulombic force are neglected. This is not to say that the Pauli Exclusion principle is not applied. Furthermore, the Coulomb interaction between the electrons and the positive protons are neglected as well. So in the free Electron Model, the electrons are free to move throughout the material subject to no Coulombic forces. Drude proposed that the electrons in this model exhibit gas like behavior and therefore the electron cloud is refereed to as a Fermi Gas of electrons [Ashcroft and Mermin, 1976]. The assumption that the electrons are "free" is a complicated matter. As my solid state physics professor once said, a free electron is similar to a free citizen "'no man is an island". So, although this is a useful model, no electron is really free and other considerations must be applied.

Solving the classic quantum mechanics problem of an electron confined to an infinite well we find that the electrons take on discretized energy levels. These energy levels are dependent upon quantum numbers indicating the shell, orbital and spin state of the electron. Free electrons in a solid fill up these energy levels maintaining two electrons per orbital. In the ground state, or the electronic configuration at absolute zero, electrons fill the lowest energy levels until all electrons are accommodated. The atomic orbitals are filled accordingly until there is a boundary where occupied states are separated from unoccupied states. The energy of the topmost filled level is defined as the Fermi Energy. In the Fermi Gas approximation the Fermi surface at absolute zero in momentum space is a sphere. The volume of the sphere encloses occupied states whose surface is the Fermi energy. At absolute zero the electrons follow a Fermi-Dirac Distribution

$$f(\epsilon) = \frac{1}{e^{\frac{(\epsilon-\epsilon_F)}{k_B T}} + 1} \tag{1.1}$$

where k_B is the Boltzman constant, T is temperature, ϵ is the energy and the chemical potential μ is equal to the Fermi energy, ϵ_F at absolute zero. As the temperature is increased, some energy levels which were vacant become filled. This eventually poses the limit for this model. Since by this model all materials are characterized by this behavior the model has no way of distinguishing between a metal and an insulator.

Heat Capacity

The first law of thermodynamics tells us that at either fixed pressure, or fixed volume a change in heat will result in a change in temperature dependent upon the type of material. The relationship between the change in heat and the change in temperature is given by the extensive physical property, heat capacity. Heat capacity scales with the size of the sample. Therefore, it is useful to work in terms of specific heat, heat capacity normalized by the mass of the material. Specific heat is an intensive or intrinsic characteristic of the material.

Classically the energy, E, of an ideal gas is given by the equipartition theorem,

$$E = \frac{3}{2} k_B T \tag{1.2}$$

where k_B is the fundamental Boltzmann constant. An elegant and simple expression for the heat capacity is derived from Equation 1.2. The Dulong - Petit Law for heat capacity, C, says

$$C = \frac{\partial E}{\partial T} = \frac{3}{2} k_B \tag{1.3}$$

This expression does not hold for low temperature heat capacity, and at room temperature the classical expression is a gross overestimation! The discovery of the Pauli

Exclusion Principle and the Fermi Distribution function solved this problem Kittel [1995]. As a system's temperature is increased from absolute zero, the electron's energies do not increase uniformly as $\sim k_B T$, rather only electrons within an energy range $k_B T$ of the Fermi level are thermally excited. So, instead of all the electrons gaining energy, a fraction of the electrons, on the order of T, can contribute to the electronic heat capacity [Gweon, 2010]. Therefore, the electronic heat capacity is given by

$$C_{electronic} = \frac{1}{3}\pi^2 D(\epsilon_F) k_B^2 T = \gamma T \tag{1.4}$$

where $D(\epsilon_F)$ is the density of states at the Fermi energy and γ is the Sommerfeld parameter. The specific heat parameter γ can tell us about the effective mass of the electrons due to the interaction with the lattice, phonons and other electrons [Kittel, 1995]. Normal metals have γ on the order of 1 $\frac{mJ}{mole}K^2$. Large gamma values are an indication of frequent electron scattering and electron drag in the material. This is accounted for by an increase in effective mass. Materials with γ on the order of 1000 $\frac{mJ}{mole}K^2$ are heavy fermion systems. The valence electrons interact strongly so they cant move around as much, so the Coulomb force becomes a much larger effect in these materials. For these materials the free electron model does not hold, but we can consider the effective heavier quasiparticles as free.

The phonon contribution to heat capacity is explained by Debye's T^3 law. Debye considered the statistical mechanics of the acoustical phonons at low temperatures which are universal among matter [Gweon, 2010]. Then the total heat capacity is given by

$$C = \gamma T + \beta T^3 \tag{1.5}$$

a the sum of the electron and phonon contributions.

Resistivity

Current I flowing through a material is proportional to a voltage drop V along the material by a factor R, this is Ohm's Law and it is given by

$$V = \frac{I}{R} \tag{1.6}$$

where R the resistance of the material. The resistance scales with the dimensions of the sample, so a more meaningful property of a material is the resistivity. Resistivity is how strongly a material opposes the flow of current. Resistivity is an intrinsic quantity, so it is sample size independent. The resistivity in the free electron model is given by

$$\rho = \frac{m}{ne^2\tau} \tag{1.7}$$

where m is the mass, ne is charge density and τ is the free time between collisions during which the applied electric field acts on the electron. The resistance and resistivity are related by

$$\rho = R\frac{A}{L} \tag{1.8}$$

where A is the cross sectional area of the material and L is the length. The electrical resistivity of most metals at room temperature is dominated by collisions of the conduction electrons with phonons. At temperatures close to absolute zero resistivity shows collisions with impurity atoms and mechanical imperfections in the lattice.

1.1.2 The Nearly Free Electron Model

The Free Electron Model's inability to distinguish metals from insulators led to the development of the Nearly Free Electron model. The distinguishing property of a solid is the electron's response to an applied electric field [Ashcroft and Mermin, 1976]. In the Nearly Free Electron Approximation, or Fermi Liquid approximation the periodic potentials of the ions are taken into account, but electron-electron interactions are still neglected. This approximation works because of the screening effect of inner orbital electrons and because of the Landau liquid Fermi theory [Gweon, 2010]. The theory states that the electrons become more "free" as the inter-atomic distance between atoms is lowered. This unintuitive results, is a consequence of the r^{-2} dependence of the coulomb potential which allows for the Coulomb potential to grow faster than the electrons potential energy.

The interaction of the conduction electron waves with the positive ionic cores forms continuous bands of allowed energies for the electrons. Generally, by Bloch's theorem the electronic energy levels in a solid form continuous bands of energy separated by gaps of forbidden energies, band gaps, corresponding to potential barriers [Ashcroft and Mermin, 1976].

Within the Nearly Free Electron model an insulator is defined as a material whose bands are either completely full or empty, and a metal is defined as a material that has one or more bands partially filled [Kittel, 1995]. Metals have no large gaps in the spectrum of allowed energies. This is why metals are such good conductors! In a typical metal the band is usually only partially filled up to the Fermi level. So, in order to excite an electron to a higher energy level requires little energy because there is no gap to overcome. Below the Fermi energy the electrons are bound to their parent atoms and the electrons are said

to contain energies in the valence band, when excited above the Fermi energy the electrons become unbound from the atom's nucleus and become a part of the conduction band. An example of the band configuration for metals and insulators can be found in Figure 1.1.

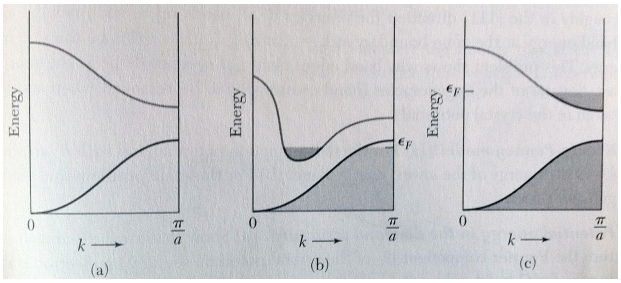

Figure 1.1: Band configuration for (a) insulators, (b) metals or semi metals and (c) metals. The gray regions are occupied states. [Kittel, 1995]

The electrical properties of a metal are determined by the volume and the shape of the Fermi surface. In this model current is due to changes in occupancy of the states near the Fermi Surface [Kittel, 1995]. The Brillouin Zone is an essential part of studying the electronic band structure of crystals. The Brillouin zone in reciprocal lattice space defines a primitive cell. Generally, the Fermi surface intersects the zone boundaries perpendicularly and the volume enclosed is dependent only on the electron concentration [Kittel, 1995]. The electronic interaction with the periodic potentials affects the Fermi surface in a few ways: the interaction creates energy gaps at the zone boundaries and the crystal potential rounds out the surface. As the crystal potential is considered the energy band of the free elections becomes narrow (the itinerant view). The other view is the localized view where each valence electron belongs to its local environment whether an atom, ion or molecule. The potentials make local states unstable, so the electrons can hop from ion to ion, exploring the crystal. Here the energy available to the electrons becomes wide. The two views come

from Bloch's theorem and are equivalent within band theory they become distinguished when electron-electron interactions are considered [Gweon, 2010].

So far both models neglected the forces between the electrons. It is when there are strong electron-electron interactions that the interesting, exotic behavior of the metals are exhibited, such as superconductivity and magnetism.

1.2 Models of Solid State Magnetism

Contrary to classical studies magnetism is a purely quantum mechanical effect. It is both a mysterious and robust phenomena that to this day is not fully understood. Applications of magnetism are both interesting and useful. Examples include your computer's hard drive, electric motors and even the core of many musical devices.

Magnetism as a macroscopic phenomena is attributed to nearest neighbor interactions on the atomic scale. A simple two particle interaction is the key ingredient to account for large scale, observed magnetic states. Magnetism is due to the magnetic moments μ of electrons given in units of Bohr Magnetons μ_B. The magnetic moment arises from an electron's angular momentum, its change in angular momentum in an applied field and its its total spin. The magnetization of a material M is defined as the magnetic moment per unit volume.

$$M = n\boldsymbol{\mu} \tag{1.9}$$

where n is the number of magnetic moments. An important dimensionless quantity, magnetic susceptibility χ, is given by the change in the magnetization with respect to an applied field,

$$\chi = \frac{\partial M}{\partial H} \tag{1.10}$$

where χ is given in CGS units and H is the applied field.

Amazingly, although magnetic moments are a quantum mechanical property they have macroscopic consequences of many different types. Magnetism can be described by: Paramagnetism, Diamagnetism, Ferromagnetism and Antiferromagnetism.

1.2.1 Paramagnetism and Diamagnetism

Materials with a positive magnetic susceptibility or positive χ given by Equation 1.10 and that only exhibit magnetism in the presence of an applied magnetic field, are said to be paramagnetic. For noninteracting atomic ions with partially filled outer shells we have the Curie's Law for paramagnetic susceptibility,

$$\chi = \frac{C}{T} \tag{1.11}$$

where C is the Curie constant. This law is derived from a thermodynamical approach to the Hamiltonian of a collection of individual ions with no interactions, $\mathcal{H} = -\boldsymbol{\mu} \cdot \mathbf{H}$ [Gweon, 2010]. Curie's Law says that at low temperatures entropy can not disrupt the spins, so spins will be aligned to the applied magnetic field, maximizing the total spin and lowering the energy of the system. As long as a magnetic field is applied at $T = 0$ all the magnetic moments will be aligned. As the temperature increases, entropy dominates and the spins will fluctuate causing spin disorder. The system enters a state of equal probability for the spins to be either up or down. Accordingly, the system will exhibit no detectable magnetic moment.

Curie's law applies to a localized view of the electrons. It explains the magnetism of transition metal ions and rare earth ions in the presence of a magnetic field. These elements tend to have valence electrons in the d and f shells, and the paramagnetic behavior is associated with the presence of those electrons. The magnetic moments in the ground state help explain the experimentally observed magnetization of these ions.

The ground state of an atom can be characterized by the total spin S, total orbital angular momentum L and total angular momentum J. These values can be calculated using Hund's rules. Hund's rules says when the d or f shell orbitals are partially filled the system will tend to maximize the total spin S. Similarly the system will try to maximize the total orbital angular momentum L. Finally, the J is given by the sum of L and S if shell is more than half full and by the difference if the shell is less than half full.

The first rule Hund's Rule is a consequence of a key force in magnetism, the exchange interaction. The exchange interaction arises from the Pauli exclusion principle, which says that electrons must satisfy a spatial symmetrization requirement dependent upon the spin of the electron because electrons can not occupy the same quantum state. Either the spin or spatial component of an electron's wavefunction must be antisymmetric. Depending on the spin state of the electrons the system will have a higher or lower Coulomb interaction. For example, if we have a symmetric spin state, both electrons have spin $\frac{1}{2}$, then the spatial state must be antisymmetric, so the electrons are farther apart. This spatial separation results in the lowering of the Coulomb potential. According to the first Hund's rule the spin is maximized, so the electrons are in the same spin state, therefore they are farther apart and the ystem will have a lower coulomb interaction. Accordingly this state is energetically favorable. Therefore, in the localized view magnetism for the transition metal

and rare earth ions is attributed to the unpaired electrons of the d and f shells electrons that like to form high spin states because the exchange interaction makes this energetically favorable state.

The localized view of an electron in matter is inadequate in describing the metallic magnetism of the transition metals, the most common materials had no theory properly explaining their properties! A more accurate description takes into account the mobility of the outer orbital electrons. These conduction electrons are partially free and should be treated a free electron gas. These electrons do not occupy energy levels dependent on orbital angular momentum. Furthermore, the orbital angular momentum is quenched by the crystal field, so the total magnetic moment is completely accounted for by the spin. Itinerant electrons in this Fermi gas approximation give rise to a weak magnetism called Pauli Paramagnetism.

A generic metal described by a Fermi gas in its ground state in the presence of an applied magnetic field in the direction to quantize spin will result in a magnetic interaction between the field and the spin of the electron. If the electron spin is aligned with magnetic field we will have a lower energy state, and if the spin is in the anti-parallel configuration we will have a higher energy state. This is reflected in two shifts in the energy bands, one associated with the spin up and another with the spin down band. The shift is quite small, $\pm\mu_B B$ on the order of a meV, whereas, Fermi energies are typically 1 eV. In this model the Fermi level does not shift, consequently one band will have more occupied states. The difference in the number of electrons in the bands results in the Pauli susceptibility. Where the susceptibility χ_0 is

$$\chi_0 = {\mu_B}^2 D(\epsilon_F) \tag{1.12}$$

proportional to the density of states on the Fermi surface $D(\epsilon_F)$ and Bohr Magneton μ_B. This is common to the coefficient of specific heat γ, and it will become important in the results section when these values are calculated directly for the Pd_2TiIn_x samples.

So, whereas localized strong magnets can align all spins because they are independent, itinerant electrons exhibit s weak paramagnetic effect because only pockets of electrons can be high spin. Pauli Paramagnetism does not depend on effective mass or band structure. Pauli Paramagnetism is purely a density of states effect at the Fermi level. [Schlesinger, 2010]

Pauli Paramagnetism is often enhanced when electron - electron interactions, band effects and diamagnetism of the ionic cores are taken into consideration. Diamagnetism is usually associated with nonmagnetic systems. As a magnetic field is applied electrons tend to create current opposing the flux change, an effect known classically as Lens law. Diamagnetism is defined as having negative magnetic susceptibility values. The enhancement of the paramagnetism is dicussed in the next section under the heading Stoner Enhancement.

1.2.2 Ferromagnetism and Antiferromagnetism

Ferromagnetism is a very strong and probably the most colloquially familiar type of magnetism. For example, iron, a classic magnet, has a large magnetic moment, and we can observe this kind of magnetism in everyday objects such as the magnets on our refrigerators. Ferromagnetic interactions occur without the help of an applied magnetic field. The system spontaneously forms long range order of the magnetic moments. Internal interac-

tions, the exchange field, line up the magnetic moments. This exchange field is higher than any field scientists can create by a few orders of magnitude. Thermal agitation can destroy the spin order, so one could try heating up a permanent magnetic at home to see at what temperature it loses its magnetization! The temperature at which this spontaneous magnetization is destroyed is known as the Curie temperature, T_C above which a paramagnetic phase dominates. The susceptibility of a ferromagnet is given by the Curie-Weiss law

$$\chi = \frac{C}{T - T_C} \tag{1.13}$$

where at $T = T_C$ the susceptibility diverges, and above T_c we have paramagnetic behavior. Recalling Equation 1.10 we see that Equation 1.13 gives finite magnetization for zero applied field. As long as the temperature is below T_C the spins will align by double exchange. In a ferromagnetic state the electron can not hop to another atom because of Pauli exclusion principle. Therefore, a ferromagnet has no higher energy state.

Antiferromagnets have a net magnetization due to oppositely magnetized lattices. Here the spins are ordered in an antiparallel arrangement with zero net moment, below T_C. At the critical temperature the susceptibility of an antiferromagnet is not infinite like the ferromagnetic case, but there is a weak cusp in the susceptibility as a function of temperature. The spins do not cancel each other out completely, so a net magnetization is observed. Antiferromagnetism is a special case of a ferrimagnet where the two sublattices have equal magnitude in the magnetization.

Examples of antiferromagnetics include Mott Insulators. A Mott insulator is collection of atoms in the limit of a large lattice constant, or large coulomb interaction. In Mott insulators two electrons occupying the same site is very energetically unfavorable, so

each site is occupied by one electron in the ground state. The true ground state has one spin flip this is the antiferromagnetic state. In the macroscopic view there is no magnetic order. In the higher energy state the electron hops or tunnels to a neighboring site. Such a state is very energetically unfavorable, and only possible for an antiferromagnet.

1.2.3 Stoner Enhancement and Spin Fluctuations

The itinerant treatment of Pauli Paramagnetism later evolved into the Stoner Model. In the Stoner Model the electrons are not localized, but are free to move within the periodic potentials of the atoms. Three postulates of the Stoner model state that the magnetic carries are the spins in the d band and that Fermi statistics must be obeyed [Fay and Appel, 1979]. It is a successful model at absolute zero, but not an accurate description at finite temperatures. The theory applies quite well to very weak itinerant systems, but it fails to predict the paramagnetic state above T_C where local moments still exist despite the breakdown in long range order. The pitfalls of the Stoner model were resolved by Moriya who suggested a collective excitation, multiple spin excitation, rather than a single particle excitation.

In the Pauli Susceptibility case there is a split in energy bands, for the up and down spins. If electron - electron interactions are introduced, this time the Fermi level will be shifted, exaggerating the occupancy discrepancy between the bands. There will be a preponderance in one band, and the band with more electrons is favored because it lowers the interaction energy.

In Stoner enhancement electron-electron interaction are reminiscent of ferromagnetism, where electron-electron interactions create spontaneous magnetism. In between

ferromagnetism and a normal metal with no interactions there is a whole range of enhancements of χ. The system tries to find a configuration in between ferromagnetism and Pauli paramagnetism. Spin fluctuation theory for itinerant electrons helps us to understand a broad range of magnetic materials.

1.3 Heusler Alloys and Pd_2TiIn_x

Heusler alloys have been studied for over a century. In 1903 Heusler found that the alloy Cu_2AlMn orders ferromagetically even though its constituent elements exhibit paramagnetic or diamagnetic behavior [Heusler et al., 1903]. This remarkable result was the first in a series of Heusler alloys. Since then Heusler alloys have been reported with group III, IV and V substitutions. One such polycrystalline intermetallic, Pd_2TiIn, crystallizes in a Heusler $L2_1$ structure. Whose elements Palladium and Titanium exhibit paramagnetic behavior and Indium exhibits diamagnetic behavior.

The $L2_1$ Heusler Alloy is a compound composed of three metallic elements with a 2:1:1 ratio. The elements crystallize in a face-centered cubic lattice as illustrated in Figure 1.2. There has been a general interest in both the Heusler structure and the half Heusler structure for some time. Many topological insulators, a hot topic in current condensed matter physics, are found to crystallize in the half-Heusler structure. Heusler alloys have also been used as a tool to study transition metal magnetism.

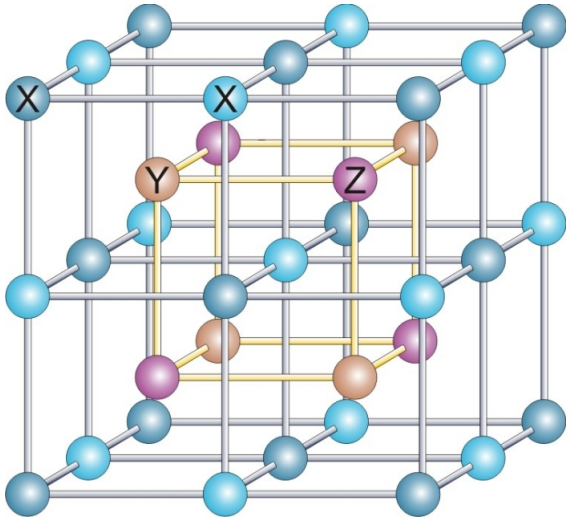

Figure 1.2: The Heusler $L2_1$ structure the Palladium atoms sit on the X sites, and the Y and Z sites are occupied by Titanium and Indium respectively. Image source: *http* : *//en.wikipedia.org/wiki/Heusleralloy*

There has been significant discussion over the type of magnetically ordered state exhibited by Pd_2TiIn. Neumann et al. [1993] report that Pd_2TiIn orders below 110K with a static susceptibility below that temperature and a localized paramagnetic moment, $\mu_p = 4\mu_B$. This is a relatively high transition temperature as compared with other weak itinerant magnets. Powder neutron diffraction measurements reported by Ouladdiaf et al. [1994] indicate a first order structural transition at 92K with no long-range magnetic order below 92K. They propose the existence of a ferrimagnetic state. Jezierski et al. [1995] confirmed that Pd_2TiIn is not ferromagnetic, but the antiferromagnetic state was not studied.

My work seeks to improve the scientific understanding of magnetism and atomic interactions in a series of polycrystalline samples derived from the inter-metallic compound Pd_2TiIn_x. The focus of this experiment was on how Indium doping effects the magnetic ordering of the Heusler alloy. In the indium-doped alloys, some percentage of the titanium

or palladium were substituted for by indium ions when the crystals were grown. Therefore some percentage of the lattice sites normally occupied by the palladium or indium atoms are instead occupied by an indium ion. Our measurements of the magnetic susceptibility, resistivity and heat capacity give insight into the band structure and magnetic ordering.

2

Experiment

By performing a series of temperature dependent measurements on the physical and magnetic properties we identified key features and characteristics of the samples as well as the relationship to Indium content. Resistivity, magnetic susceptibility and low temperature heat capacity were measured as a function of temperatures from 2 - 300K, using two sophisticated measurement systems described in the sections below.

2.1 Pd_2TiIn_x Samples

Six polycrystalline Pd_2TiIn_x samples with Indium concentrations $0.87 \leq x \leq 1.22$ were prepared by Callie Oglesby. The buttons were arc welded on a copper hearth using high purity powders in an argon atmosphere. X-ray diffraction measurements on the samples performed by Theo Seigrest confirmed the Heusler L21 structure at each composition a table of the lattice parameters at each composition is given in Table 2.1. The distance between the Ti atoms in a Heusler structure is given by $\frac{a}{\sqrt{2}}$.

x	a
0.87	6.38984 ±0.0116
0.93	6.39601 ±0.0116
1	6.39877 ±0.0116
1.12	6.40433 ±0.0116
1.17	6.4136 ±0.0116
1.22	6.40774 ±0.0116

Table 2.1: The lattice parameter a given in units of Åas a function of indium doping x

Heat capacity and resistance measurements were made using the Physical Properties Measurement System (PPMS) manufactured by Quantum Design. AC Susceptibility measurements were made on a Magnetic Properties Measurement System (MMPS) again manufactured by QD. Measurements were taken at temperatures between 2 - 300K with an applied magnetic field.

2.2 Magnetic Properties Measurement System (MPMS)

The MPMS measures the voltage induced as the sample traverses the sample chamber. As the sample moves up the lowest coil its magnetic moment induces a positive voltage, as it moves through the center coils wound in the opposite direction a negative voltage is induced finally as it passes through the top coil a positive voltage is induced. The sample then moves down the chamber and the process is repeated.

Magnetization measurements were performed using the Magnetic Properties Measurement System (MPMS) magnetometer manufactured by Quantum Design. The MPMS is a variable temperature, sensitive magnetic moment detection system. It is computer controlled and allows for real time viewing of the data. Large magnetic fields, $\pm 7 Tesla$,

are produced by the Superconducting Quantum Interference Device (SQUID). The SQUID can then detect changes in the field which are 14 orders of magnitude smaller [McElfresh, 1994]. A schematic illustration of the MPMS can be found in Figure 2.1. The SQUID is immersed in a vessel of liquid helium and surrounded by a vacuum. It can achieve temperatures as low as 1.9K. The detection coil is thermal isolated from the sample chamber to allow the chamber temperature to be varied. The coil is immersed in a helium bath outside the sample chamber, and detect the magnetic moment of the sample as it moves up and down the sample chamber. A measurement is performed by stepping the sample through the detection coils. The detection coil is a second order gradiometer composed of a single superconducting wire wound in a set of three coils. The samples magnetic moment induces a current in the coil. A current to voltage converter produces an output voltage proportional to the magnetic moment which in turn determines the materials magnetization and then magnetic susceptibility. A fixed DC field is applied as the sample is moved into the detection coils region of sensitivity. They have a homogeneous superconducting magnet to create a very uniform field over the entire sample measuring region and the superconducting pickup loops. The magnet induces a moment allowing a measurement of magnetic susceptibility. The detection coil geometry determines what mathematical algorithm is used to calculate the net magnetization. The induced current is independent of the rate of flux change allowing for slow sample movements through the chamber. As the sample passes through a coil, it changes the flux in that coil by an amount proportional to the magnetic moment of the sample. The peak-to-peak signal from a complete cycle is thus proportional to twice the moment. The coils are wound in a way which strongly rejects interference from nearby magnetic sources and lets the MPMS function without a superconducting shield around the

pickup coils.

For materials that might not be characterized as magnetic applying a field can reveal information about electronic structure, interactions between neighboring molecules or the character of a transition between phases of the material. If the sample doesnt have a permanent magnetic moment, a DC field is applied to induce one.

The measurement procedure involves mounting a sample to the end of a rigid rod that is inserted into the sample chamber. The chamber is air-locked and a vacuum is pulled to within a few torr. The sample is then driven up and down the squid detection coils in discrete steps to generate a change a flux. Several reading of the SQUID voltage are taken and then averaged by the equipment's software.

The magnetic moment calibration for the SQUID is determined by measuring a palladium standard over a range of magnetic fields and then by adjusting to obtain the correct moment for the standard. The palladium standard samples are effectively point sources with an accuracy of approximately 0.1% [Design, 2004].

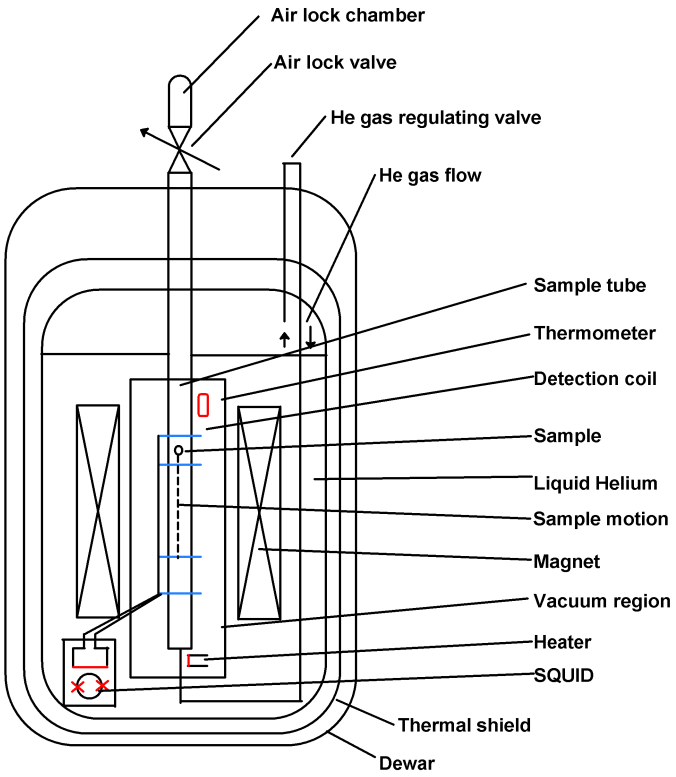

Figure 2.1: A schematic diagram of the Magnetic Properties Measurement System. [Author, 2011]

Magnetic Susceptibility Measurements

Materials with a low magnetic susceptibility where chose to mount the samples. This is done to keep the contribution to the background signal at a minimum. The samples are enclosed within a gelatin pill capsule and secured with cotton to minimize torquing in the magnetic field. The pill capsule is held inside of an ordinary plastic drinking straw and cross threaded into place using fishing line as shown in Figure 2.2. The straw, cotton and pill capsule are lightweight and perform well over a large temperature range. The samples weighed approximately 20 - 100 mg and the geometric arrangement of the samples was not critical as they were polycrystalline.

To ensure that all coils sense the magnetic moment of the sample we perform a centering scan that ensures th sample is centered in the SQUID pickup coils. If the sample is not centered, the coils read only part of the magnetic moment. During a centering scan the MPMS scans the entire length of the samples vertical travel path. The sample moves upward, carrying the sample through the pickup coils, then the MPMS brigs the sample down through the coils. While the sample moves through the coils, the MPMS measures the SQUIDs response to the magnetic moment of the sample and saves all the data from the centering measurement. The voltage readings are plotted as a function of position, and examined to determine whether the sample is centered in the SQUID pickup coils. The sample is centered when the part of the large, middle curve is within 5cm of the half-way point of the scan length McElfresh [1994].

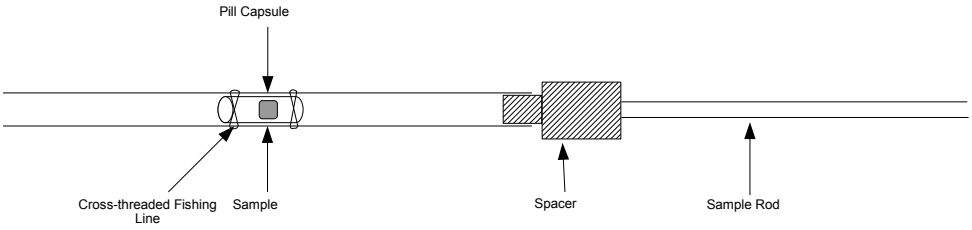

Figure 2.2: A schematic diagram of a sample mounted for measurement in the MPMS.

2.3 Physical Properties Measurement System (PPMS)

Resistivity and heat capacity measurements were performed using the Physical Properties Measurement System (PPMS) manufactured by Quantum Design. The PPMS is a liquid

helium cooled, temperature and field variable system capable of doing a number of thermal and electrical measurements. The system can generate magnetic fields between ±7 Tesla and temperatures between 1.9 and 400K. It is computer controlled and data can be viewed via a computer in real-time. The PPMS is composed of a standard dewar with a liquid helium bath in which a probe is immersed. The probe is capable of temperature control and is composed of a superconducting magnet, a sample puck connector and electrical connections. The sample chamber is inside a vacuum tube base has 12-pin connector that connects to sample puck. a vacuum pump continuosly pumps sample chamber.

Resistance Measurements

Samples were cut into long thin rectangular bars for a standard four wire DC resistance measurement They were cut using a diamond impregnated wire saw. The samples were then polished using fine sand paper and four silver epoxy contacts were baked on the samples, a pair of contacts at the ends of the bar (see Figure 2.3). The silver epoxy created electrical contact with gold wires that attached to leads on a sample puck that connected to pins of the PPMS probe. The sample puck is a copper, gold-plated disk with a 2.3 cm diameter. Thermometers and heaters are directly below the sample puck when it is installed in the sample chamber. One puck can accommodate 3 samples. Each lead and sample was electrically, but not thermally isolated using ordinary cigarette paper. Current was fed through two electrical leads placed at the very ends of the sample and the two inner leads measured the potential drop across the sample. The input impedance of the the voltmeter used allowed for a high degree of accuracy for the resistance value measured [Design, 2000]. Proper Electrical connections were verified using a digital voltmeter before the sample was

installed into the chamber. Once the puck was installed the sample chamber was purged and sealed and resistivity measurements were taken at 0 Tesla and at an applied field of 7 Tesla over the temperature range from 2 K - 300 K. Using the geometry of the samples the data were further processed to obtain resistivity values as discussed in the Results.

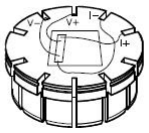

Figure 2.3: A schematic diagram of a four wire resistance measurement with the sample mounted on a PPMS sample puck electrically isolated with cigarette paper.

Heat Capacity Measurements

Heat capacity at low temperatures, well below the DeBye Temperature, directly probes the electronic and magnetic energy levels. The PPMS measures heat capacity using the two tau model and relaxation method. The heat capacity option measures heat capacity at constant pressure by applying a known amount of heat for a fixed time followed by a cooling period of the same amount of time. After each heating and cooling cycle, the system takes one measurement. The relaxation technique fits the temperature response of the platform and accounts for the thermal relaxation of the platform to the bath and the relaxation between the platform and the sample. An addenda measurement is taken of the sample puck and a small amount of grease. The PPMS automatically subtracts the addenda measurement from a heat capacity measurement leaving you with the heat capacity of the sample. The PPMS Heat capacity option uses a different puck that requires the sample to have thermal contact to a platform placed in a copper heat bath. The platform has four wires connected to a thermometer and a heat source to measure heat capacity. Because the sample expands

and contracts it is important to have very good coupling with the sapphire platform. This is achieved by polishing our samples so they have a flat surface and ensuring contact with the platform using Apezion grease. The puck has a thermal radiation shield, and a turbo pump is used to pull a sufficient vacuum about 1 mtorr. A charcoal holder is used as a cryopump in the vicinity of the sample to ensure that the local pressure is low. Poor thermal coupling to the platform is indicated by the PPMS as a sample coupling percentage. Samples with data coupled less than 90% were always remounted and remeasured to maintain good quality data.

3

Results

3.1 Magnetic Susceptibility

The data are outputted by the MPMS in the form of a table consisting of the applied magnetic field, temperature of the sample, and the measured magnetic moment. A section of the datasheet for Pd_2TiIn is shown in Table 3.1.

Field (Oe)	Temperature (K)	Long Moment (emu)
5000	2.2	0.00110
5000	2.49	0.00109
5000	2.8	0.00108
5000	3.1	0.00107
5000	3.4	0.00107
5000	3.7	0.00107
5000	3.99	0.00106
5000	4.29	0.00106
5000	4.6	0.00106
5000	4.9	0.00106
5000	5.2	0.00105
5000	5.5	0.00105
5000	5.8	0.00105
5000	6.1	0.00105
5000	6.4	0.00105
5000	6.7	0.00104
5000	7	0.00104
5000	7.3	0.00104
5000	7.6	0.00104
5000	7.9	0.00104
5000	8.2	0.00104
5000	8.5	0.00104
5000	8.8	0.00104
5000	9.1	0.00104
5000	9.4	0.00104
5000	9.71	0.00103
5000	10	0.00103
5000	10.01	0.00104

Table 3.1: Example of the MPMS output data for Pd_2TiIn in the range of 2.2 - 10K

To calculate the magnetic susceptibility of the sample we use a modified version of Equation 1.10. Scaling the magnetic moment by the sample mass and molar mass. Then we divide the magnetization by the applied field to obtain

$$\chi = \frac{M}{H}\frac{m_{molar}}{m} \tag{3.1}$$

where m is the mass of the sample and m_{molar} is the molar mass. The susceptibility is the plotted per mole of Palladium and as a function of temperature. The susceptibility data for the stoichiometric sample Pd_2TiIn in a temperature range of 2 - 300K with an applied field of 0.5 Tesla is shown in Figure 3.1.

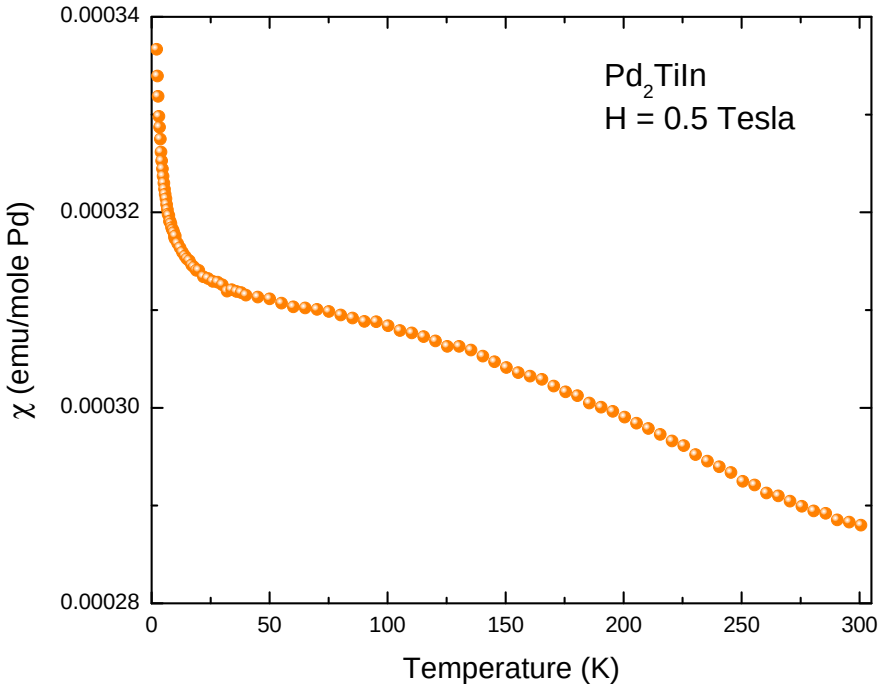

Figure 3.1: Magnetic Susceptibility data of Pd_2TiIn in a temperature range of 2 - 300K with an applied field of 0.5 Tesla.

At low temperatures the magnetic susceptibility of the series begins to diverge following curie susceptibility behavior Equation 1.11. This behavior is attributed to the magnetic impurities found in the sample. We fit the data to the Curie susceptibility and remove the inverse T contribution. If the whole tail is due to a single spin $\frac{1}{2}$ on a Palladium site randomly oriented due to defects, it is less than 1% per mole Palladium. Once the Curie

Tail due to magnetic purities are removed the true physics of the samples can be identified. The corrected susceptibility is then plotted as a function of temperature as shown in Figure 3.2. This procedure is done for each sample in the series. A plot of the susceptibilities for all the samples is shown in Figure 3.3.

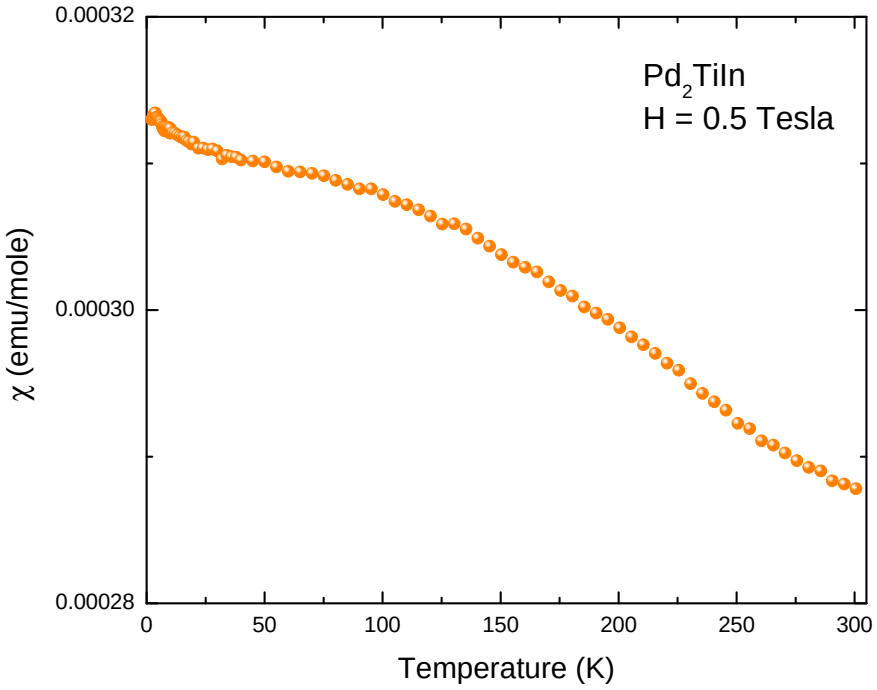

Figure 3.2: Magnetic Susceptibility data of Pd_2TiIn in a temperature range of 2 - 300K with an applied field of 0.5 Tesla with the Curie susceptibility subtracted out.

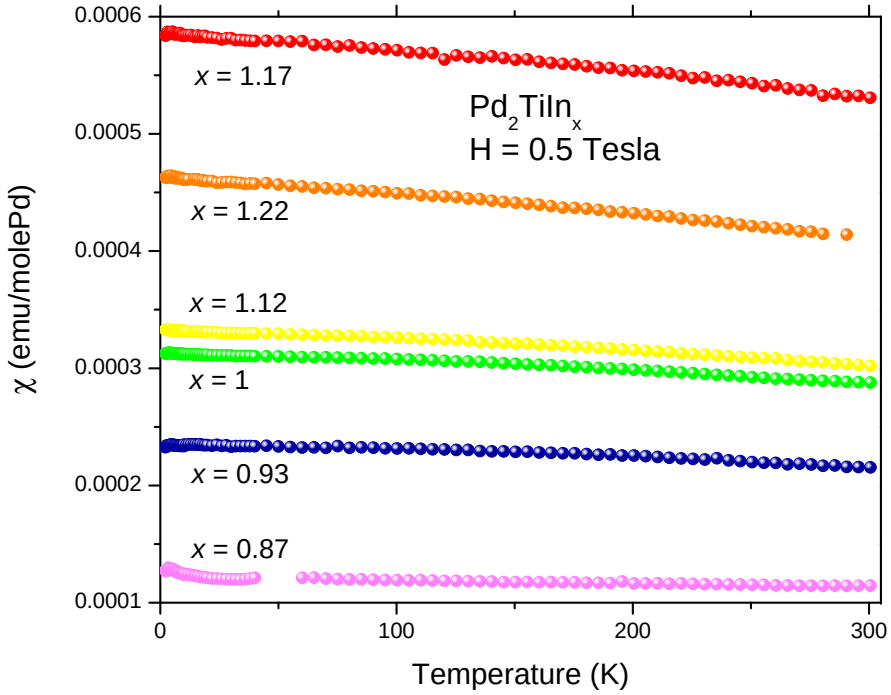

Figure 3.3: Magnetic Susceptibility data of Pd_2TiIn_x series in a temperature range of 2 - 300K with an applied field of 0.5 Tesla with the Curie susceptibility subtracted out.

There was some oxygen contamination in a few samples characterized by a sharp peak at 43K, the temperature at which molecular oxygen undergoes an antiferromagnetic transition [Design, 2011]. We repeated the measurements ensuring that all the faulty seals were replaced and that the sample were properly outgassing during the airlock process. For this reason one data point from $Pd_2TiIn_{0.87}$ is missing.

3.2 Heat Capacity

The PPMS outputs heat capacity data in the form of a table consisting of the sample temperature, sample heat capacity, sample heat capacity divided by temperature and tem-

perature squared. A section of a datasheet measuring Pd_2TiIn is shown in Table 3.2.

Temperature (K)	$C_P(\frac{mJ}{moleKPd})$	Temperature^2 (K^2)	$\frac{C_P}{T}(\frac{mJ}{moleK^2Pd})$
3.49	9.95	12.17	13896.63
3.49	9.97	12.18	13909.91
3.49	9.98	12.19	13913.68
3.21	8.44	10.33	12783.01
3.22	8.47	10.34	12827.94
3.22	8.44	10.35	12771.98
2.96	7.2	8.74	11857.99
2.96	7.19	8.74	11847.59
2.96	7.19	8.76	11835.08
2.72	6.21	7.41	11102.77
2.72	6.2	7.42	11080.55
2.73	6.22	7.43	11112.29
2.51	5.41	6.28	10521.1
2.51	5.42	6.28	10528.61
2.51	5.42	6.29	10527.52
2.31	4.83	5.32	10195.65
2.31	4.77	5.32	10082.28
2.31	4.78	5.32	10084.31
2.12	4.14	4.49	9508.24
2.12	4.14	4.5	9510.2
2.12	4.13	4.5	9488.45

Table 3.2: Example of the PPMS datasheet for Pd_2TiIn for the Heat Capacity Experiment

To calculate the specific heat of the sample we multiply the sample heat capacity by the molar mass, m_{molar}, and divide by the sample mass, m.

The specific heat was then plotted as a function of temperature for the stoichiometric sample as shown in Figure 3.4.

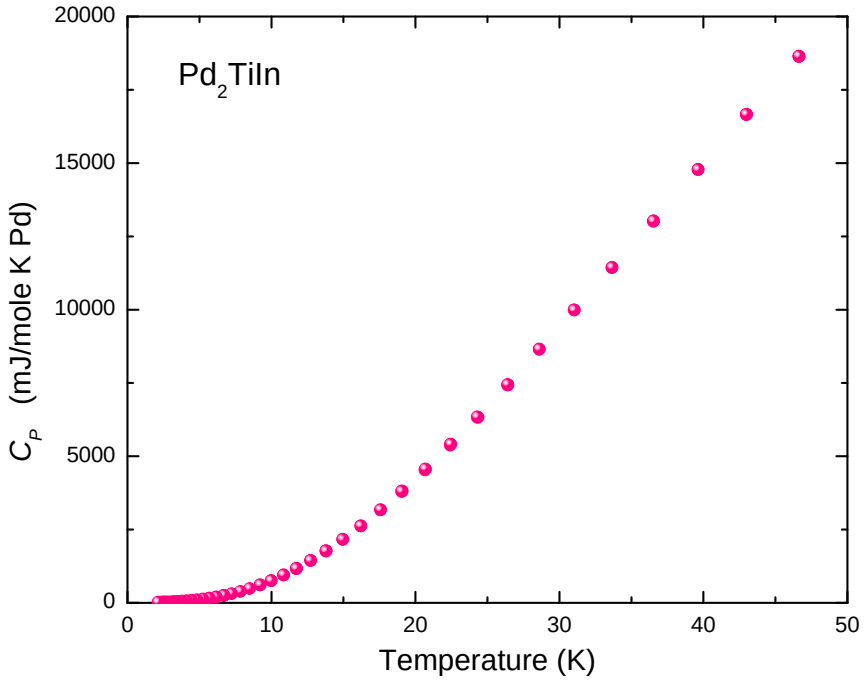

Figure 3.4: Heat Capacity data for Pd_2TiIn in a temperature range of 2 - 50K.

Experimentalists often find it convenient to write Equation 1.5 as

$$\frac{C}{T} = \gamma + \beta T^2 \tag{3.2}$$

this is done because the data points lie on a straight line with slope β and y - intercept γ as shown for Pd_2TiIn in Figure 3.5. This procedure was done for each sample in the series. A plot of the specific heat for all the samples is shown in Figure 3.6.

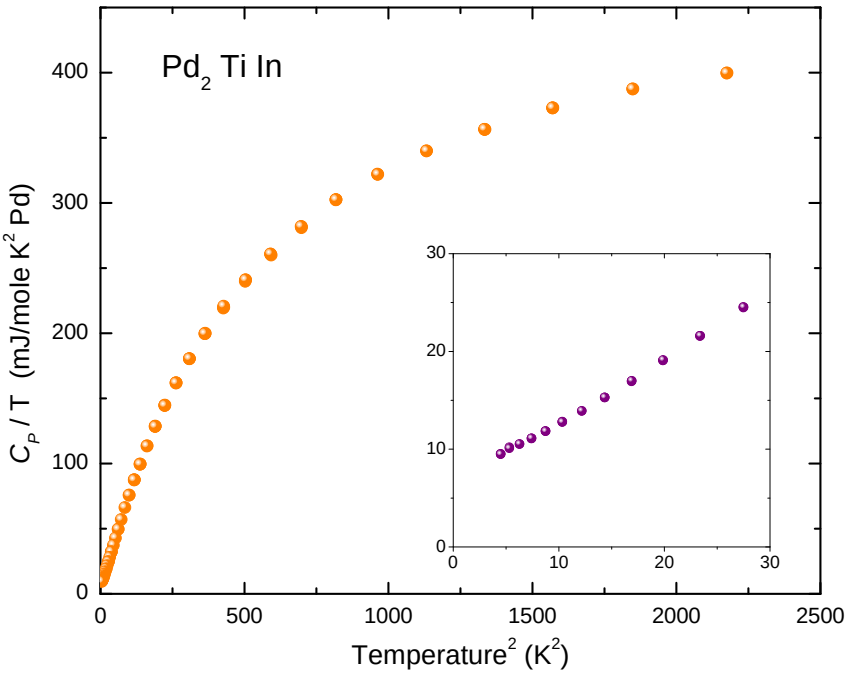

Figure 3.5: Heat Capacity data for Pd_2TiIn as a function of T^2. The inset shows the low temperature linear behavior electronic contribution to the heat capacity.

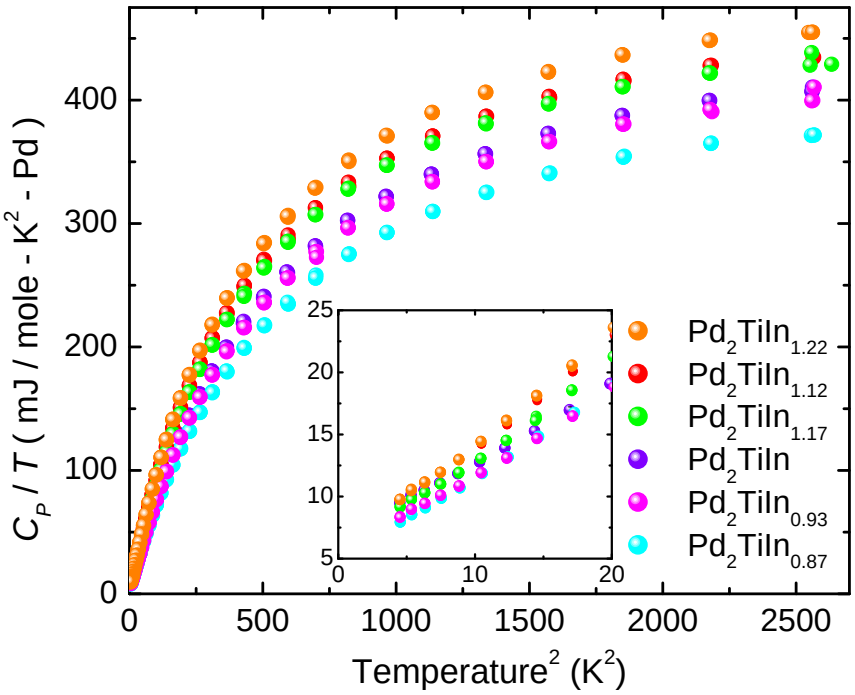

Figure 3.6: Heat Capacity data of the series Pd_2TiIn_x as a function of T^2. The inset shows the low temperature linear electronic contribution to the heat capacity.

3.3 Resistance

The PPMS outputs resistance data in the form of a table consisting of the sample temperature and sample resistance. The samples were measured with an applied field did not differ from that with an applied field in a temperature range of 2K - 300K. Only data without an applied field are presented. A section of a datasheet is shown in Table 3.3.

Temperature(K)	Field (Oe)	Resistance (Ω)
10.04	0.09	0.01833
11.46	0.09	0.01832
12.92	0.09	0.01833
14.37	0.09	0.01833
15.83	0.09	0.01834
17.29	0.09	0.01836
18.75	0.09	0.01836
20.2	0.09	0.01836
21.66	0.09	0.01835
23.12	0.09	0.01836
24.58	0.09	0.01837
26.03	0.09	0.01837
27.49	0.09	0.01837
28.95	0.09	0.01837
30.41	0.09	0.01838
31.87	0.09	0.01837
33.32	0.09	0.01836
34.78	0.09	0.01837
36.23	0.09	0.01836
37.69	0.09	0.01836
39.15	0.09	0.01836
40.6	0.09	0.01836

Table 3.3: Example of the PPMS output data for Pd_2TiIn for the Resistivity Experiment

To calculate the resistivity of the sample the dimensions of the sample were measured and Equation 1.8 used. The resistivity was then plotted as a function of temperature for the stoichiometric sample as shown in Figure 3.7.

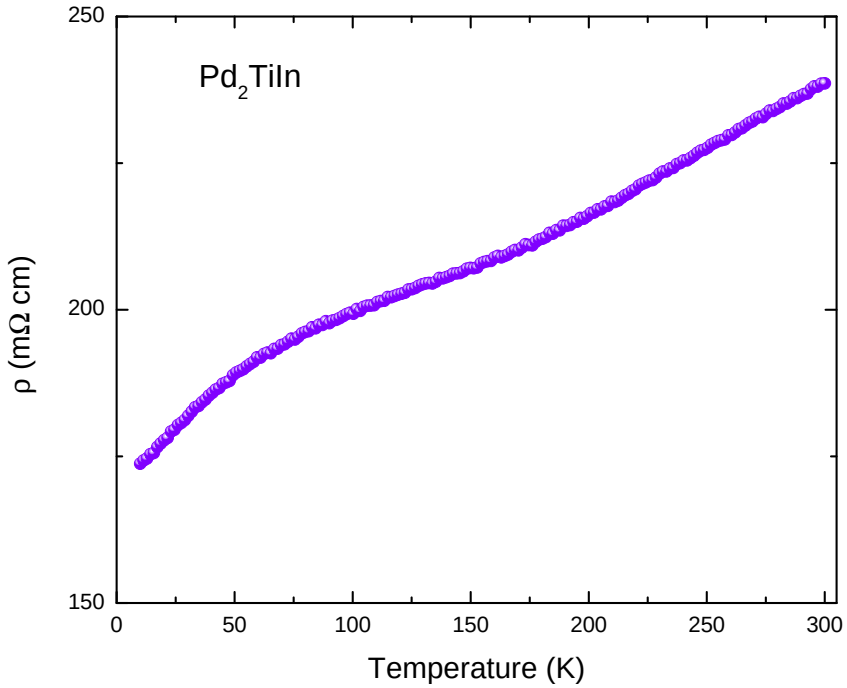

Figure 3.7: Resistivity data for Pd_2TiIn in a temperature range of 2 - 300K

The resistivity was then plotted as a function of temperature for all the samples as shown in Figure 3.8.

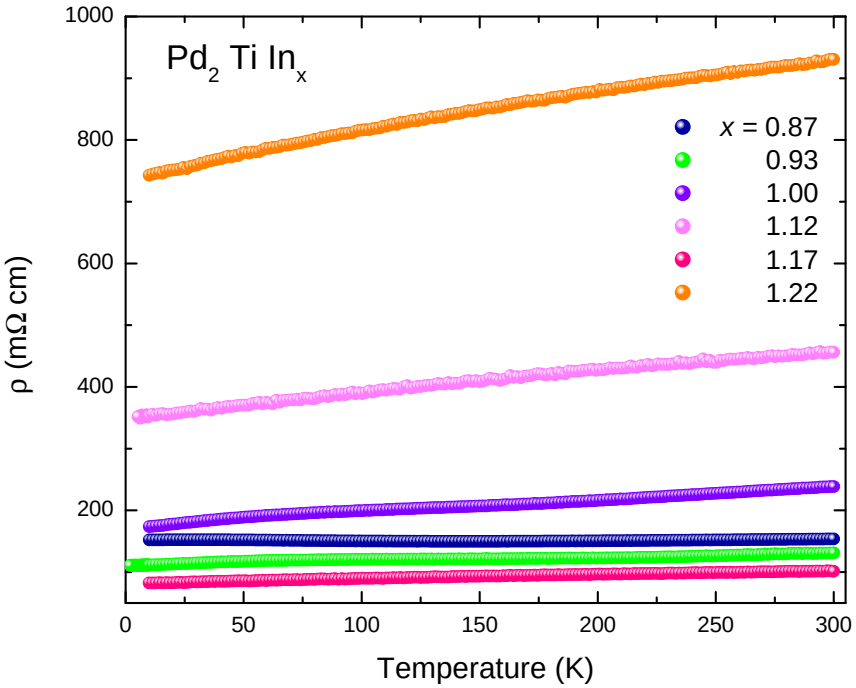

Figure 3.8: Resistivity data for the Pd_2TiIn_x series in a temperature range of 2 - 300K

4

Analysis and Conclusions

The data from the results were analyzed used fitting functions to extract useful parameters. The procedure, fitting functions and parameter significances are discussed below.

4.1 Magnetic Susceptibility

The low temperature susceptibility approached a constant value χ_0 as the temperature decreased toward 0K. χ_0 was extracted by a fitting function using OriginLabs 6.1 to determine the Pauli Paramagnetism as shown in Figure 4.1. The values for χ_0 at each composition are plotted as a function of indium content in Figure 4.5.

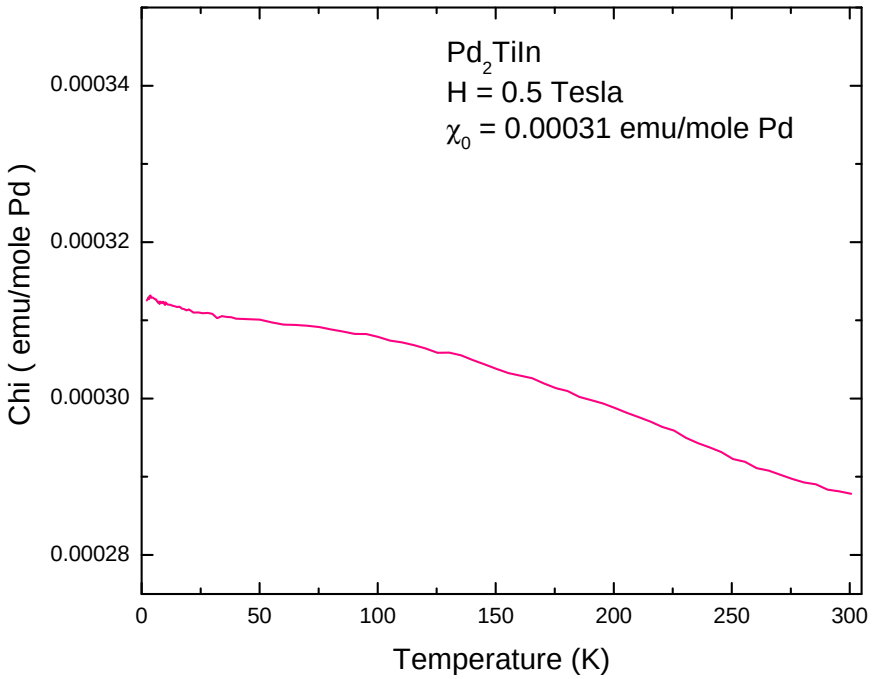

Figure 4.1: Fitted Magnetic Susceptibility Data for Pd_2TiIn

4.2 Heat Capacity

The electronic contribution to the heat capacity is deduced by plotting the data, as in Equation 3.5 and extrapolating the data linearly below $\sim$ 5K to the y-intercept, as shown in Figure 4.2. The linear fit of the data yields a γ value as discussed in the Introduction. The values for γ at each composition are plotted as a function of indium content in Figure 4.5.

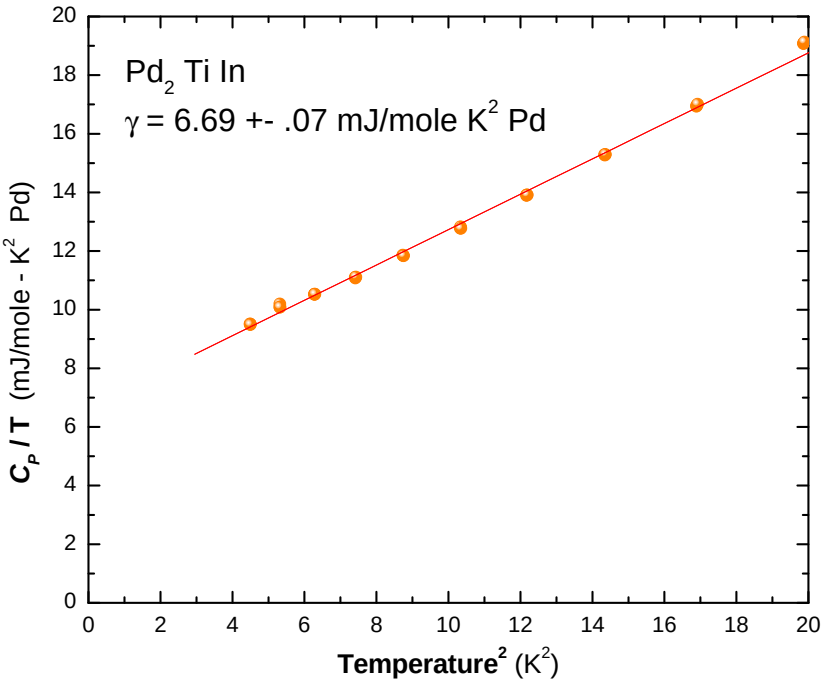

Figure 4.2: Low temperature electronic Heat Capacity for Pd_2TiIn. The red line is a linear fit extrapolated to the y-axis to deduce γ.

4.3 Resistivity

The resistivity curves were all fit to a function of the form

$$\rho = \rho_0 + \rho_1 T + Ae^{-\frac{T-T_C}{2\omega}^2} \tag{4.1}$$

where ρ_0 is the residual resistivity, ρ_1 is the linear contribution to the resistivity and T_C the transition temperature. The residual resistivity ρ_0 is the extrapolated resistivity at absolute zero. The resistivity data and fitting functions are plotted in Figure 4.3. The stoichiometric and low doped samples are plotted separately in Figure 4.4 to highlight

the presence of the Gaussian peaks by normalizing the data and the extracting just the peak from the data. The resistivity curves (Figure 3.8) show an overall linear increase in resistivity with temperature, and the curves also show a pronounced Gaussian peak in the stoichiometric and under-doped samples data at low temperatures. The values for ρ_0, ρ_1, and T_C at each composition are plotted as a function of indium content in Figure 4.5.

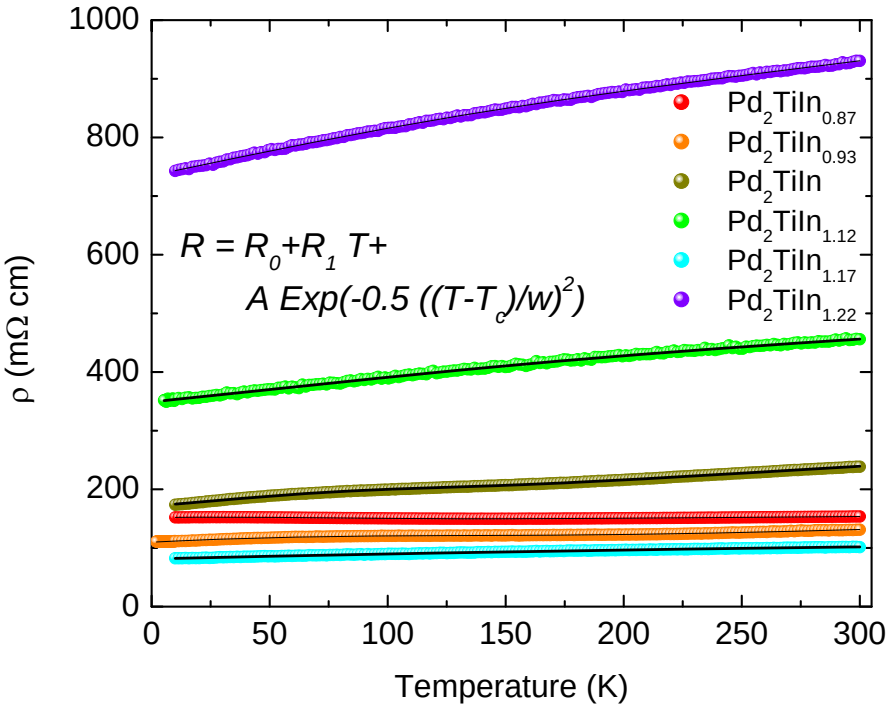

Figure 4.3: Resistivity data fit for the entire Pd_2TiIn series.

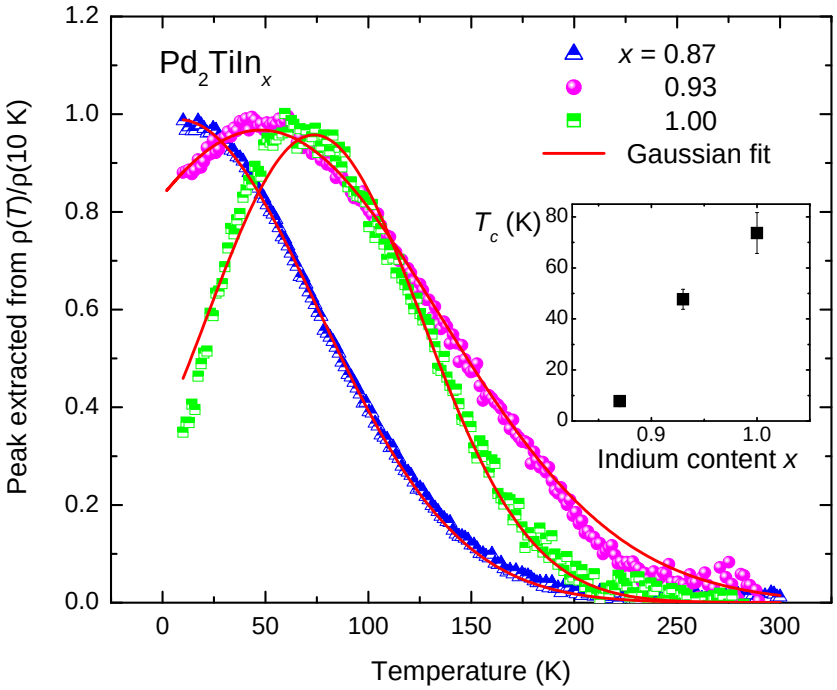

Figure 4.4: Resistivity Gaussian Peaks extracted from data, normalized and fit for the Pd_2TiIn lower doped samples. The inset shows the critical temperature as a function of Indium content.

4.4 Parameters and Wilson's Ratio

The parameters χ_0, ρ_0, ρ_1 and γ for the Pd_2TiIn_x series are plotted as a function of indium content in Figure 4.5.

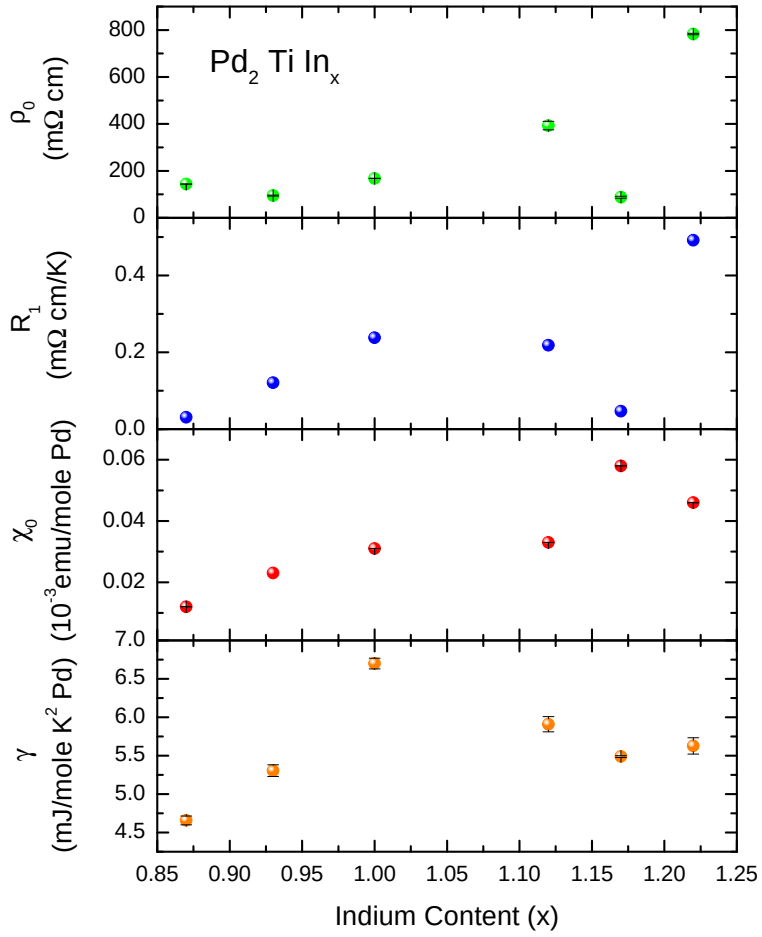

Figure 4.5: Fit Parameters for the Pd_2TiIn Series as a function of Indium for the resistivity, magnetic susceptibility and heat capacity data.

χ_0 has a strong dependence on the Indium content. As a function of indium content the Pauli susceptibility increases linearly. There are a few outliers that can be attributed to samples with impurities or without long range crystallinity. The stoichiometric and lower doped samples show an increase in transition temperature with doping, and verified that the higher doped samples do not exhibit the Gaussian term. The Resistivity drops significantly for th doped series indicating that the stoichiometric crystal has a structure and electrical

interaction that impedes flow.

The large Pauli Susceptibility and the large gamma quantity for the stoichiometric Pd_2TiIn motivated the calculation of the Wilson Ratio for the entire series. Wilson's ratio has proved to be useful in characterizing strongly correlated Fermi liquids McKenzie [1999]. The Wilson Ratio, R, relates χ_0 and γ and is defined as the dimensionless ratio

$$R = \frac{4\pi^2 k_B^2 \chi_0}{3(g\mu_B)^2 \gamma} \tag{4.2}$$

where g is the gyro-magnetic ratio in the absence of interactions [McKenzie, 1999]. A table of the Wilson's Ratio for each sample in the series can be found in Table 4.1 where Equation 4.2 reduces to R = 0.73 $\frac{\chi_0}{\gamma}$ with g = 2 and the units used as shown in the table. The Wilson's Ratio grows linearly with Indium content as plotted in Figure 4.6.

Compound	γ (mJ/(K^2 mol Pd))	χ_0 (10^{-5} emu/mol Pd)	R
Pd_2TiIn	6.7	31.0	3.38
$Pd_2TiIn_{0.87}$	4.66	12.0	1.88
$Pd2TiIn_{0.93}$	5.3	23.0	3.17
$Pd2TiIn_{1.12}$	5.91	33.0	4.08
$Pd2TiIn_{1.17}$	5.49	58.0	7.71
$Pd2TiIn_{1.22}$	5.63	46.0	5.97

Table 4.1: Wilson's Ratio R calculated from measurements of the χ_0 and γ using the units used here and g = 2 Equation 4.2 becomes $R = 0.73\frac{\chi_0}{\gamma}$

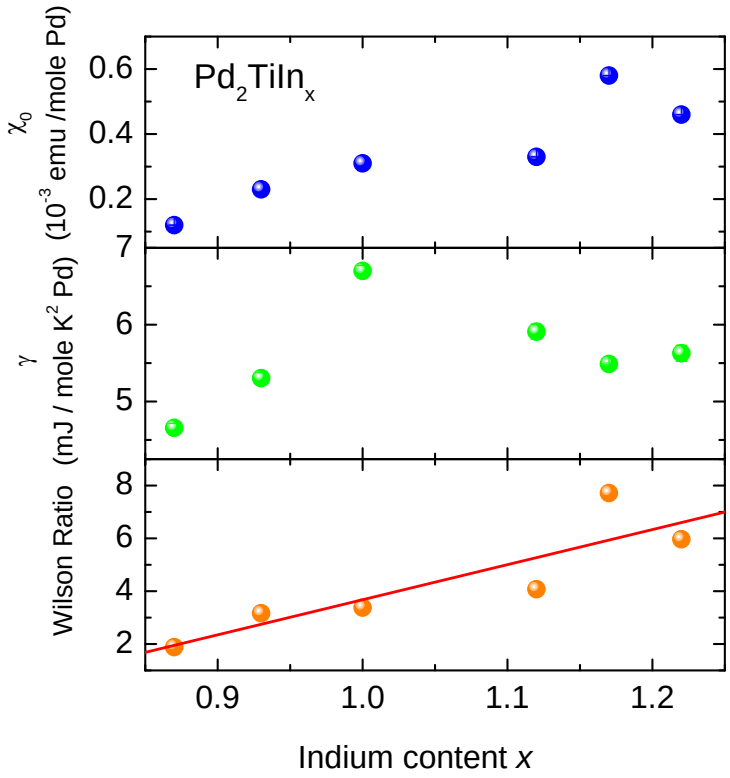

Figure 4.6: Wilson Ratio, Gamma and Chi plotted for the Pd_2TiIn_x series as a function of indium content.

4.5 Conclusions

In a Fermi gas the low temperature specific heat coefficient γ and χ_0 scale linearly with the density of states at the Fermi level. So, for a typical Fermi gas, where electron-electron interactions are negligible, Wilson's Ratio is 1. For the Pd_2TiIn_x series there is an obvious growth of the Wilson's Ratio with Indium content. The Wilson's Ratio is greater than 1,

so this is a clear indication that the density of states at the Fermi level is enhanced with Stoner Enhancement for the magnetic state of the system. Gamma changes from from 4.6 - 6 this is a 50 -40% change across the whole range. Whereas, χ_0 changes by a lot more. These changes are reflected in the Wilson's Ratio. Enhancement of the magnetization in this material is a consequence of structure of the constituent elements. There is not just a Density of State effect, but also a Stoner enhancement at the Fermi level. If the Wilson's Ratio is changing we have to have a stoner enhancement developing across the whole series. Furthermore, the Gaussian peaks in resistivity for the lower doped samples indicate an increase in the transition temperature with the Wilson's ratio. The resistivity data are also flat and high indicating that these samples can be bad metals.

Our samples were not multiply annealed this may have affected the long range crystallinity. This may be why our magnetic susceptibility data did not have peaks as pronounced as data reported from other sources. The lack of long range crystallinity does not affect microscopic energetics that are important for establishing Fermi levels. A later study would anneal the samples further to find correlation of long range order with fundamental short range properties.

Bibliography

Neil W. Ashcroft and N. David Mermin. *Solid State Physics*. Brooks Cole, 1976.

Unknown Author. Practical guide to using a squid, 2011. URL `http://cnx.org/content/m22968/latest/`.

Quantum Design. *PPMS User's Manual*. San Diego, Ca, 2000.

Quantum Design. *MPMS User's Manual*. San Diego, Ca, 2004.

Quantum Design. *MPMS Application Note: Oxygen Contamination*, 2011.

D. Fay and J. Appel. Phonon contribution to the stoner enhancement factor: Ferromagnetism and possible superconductivity of zrzn_2. *Phys. Rev. B*, 20(9):3705–3708, Nov 1979. doi: 10.1103/PhysRevB.20.3705.

Gey Hong Gweon. Solid state physics lectures, Winter 2010.

F. Heusler, W. Starck, and E. Haupt. Unknown title. *Verh. Deut. Phys.*, 1903.

A Jezierski, J A Morkowski, A Szajek, and M Pugacheva. Electronic structure in ternary intermetallic $pd_2tix(x = al, ga, in)$ heusler-type alloys: are they magnetic? *Journal of Physics: Condensed Matter*, 7(23):4447, 1995. URL `http://stacks.iop.org/0953-8984/7/i=23/a=013`.

Charles Kittel. *Introduction to Solid State Physics*. Wiley, 1995.

Mike McElfresh. Fundamentals of magnetism and magnetic measurements featuring quantum design's magnetic property measurement system, 1994.

Ross H. McKenzie. Wilson's ratio and the spin splitting of magnetic oscillations in quasi-two-dimensional metals, 1999. URL `http://www.citebase.org/abstract?id=oai:arXiv.org:cond-mat/9905044`.

K.U. Neumann, J. Crangle, R.K. Kremer, N.K. Zayer, and K.R.A. Ziebeck. Magnetic order in pd2tiin: A new itinerant antiferromagnet? *Journal of Magnetism and Magnetic Materials*, 127(1-2):47 – 51, 1993. ISSN 0304-8853. doi: DOI: 10.1016/0304-8853(93)90194-7. URL `http://www.sciencedirect.com/science/article/pii/0304885393901947`.

B Ouladdiaf, K U Neumann, J Crangle, N K Zayer, K R A Ziebeck, and E Ressouche. A neutron diffraction study of the phase transition in pd_2tiin. *Journal of Physics: Condensed Matter*, 6(8):1563, 1994. URL `http://stacks.iop.org/0953-8984/6/i=8/a=014`.

Zack Schlesinger, 2010.